Surface patterning by ripples using femtosecond laser for sensing and opto-fluidics

Ričardas Buividas[a], Daniel J. Day[a], Saulius Juodkazis[a,b]

[a]Centre for Micro-Photonics, Faculty of Engineering and Industrial Sciences, Swinburne University of Technology, Hawthorn, VIC 3122, Australia

[b]Melbourne Centre for Nanofabrication, 151 Wellington Road, Clayton, VIC 3168, Australia

ABSTRACT

Ripples on silicon have been fabricated by femtosecond laser ablation to minimize Si removal and to achieve a flat (not a groove-like) coverage of extended millimeter size areas for nano-/micro-fluidic applications. Such flat ripple-covered regions were found to control flow and wetting properties of water. Depending on orientation of ripples the flow speed of a 1 μl water droplet can be changed from 1.6 to 9.1 mm/s. Gold-coated ripples on sapphire are demonstrated as an excellent SERS substrate with more than one order-of-magnitude larger sensitivity and superior reproducibility as compared to the commercial SERS substrates; SERS signal on the ripples was more than 15 times higher and more than 2 times more uniform as compared to Klarite substrate at 633 nm excitation wavelength. It was shown that ripples can also be fabricated on thin transparent conducting indium tin oxide (ITO) coatings of 45 nm thickness. The electrical resistance can be controlled by orientation and area fraction of ripples. Applications on miniaturized heaters for incubation and micro-chemistry chambers on lab-on-chip and electrowetting are discussed along with potential applications in orientational flows, self-assembly of micro-chips, and sensing.

Keywords: ripples, lab-on-chip, femtosecond laser ablation, ITO, super-wicking surface, hydro-phobicity/philicity

1. INTRODUCTION

Surfaces covered by ripples[1,2] formed via laser ablation are finding wide range of applications in automotive industry as oil retaining areas in engine's cylinders, water repelling surfaces due to nano-texture caused change of the contact angle,[3,4] light extracting surfaces in light emitting diodes (LEDs),[5] light trapping surfaces and electrical contacts' retaining tracks on silicon for solar cell applications,[6] a wet etching of channels recorded inside dielectrics is affected by presence of ripples and can be used to speed up channel opening, etc.

Theory of ripple formation on absorbing surfaces have been established and the ripples whose wavevector is parallel (the normal ripples) and perpendicular (anomalous ripples) to the polarization of incident light are well understood as an interaction of incident and scattered light fields.[7,8] The normal ripples on silicon and metals can be explained by the proposed theory.[9–13] Subwavelength ripple formation in the bulk of dielectric or semi-dielectric materials is still strongly debated.[14–16] At the conditions close to an optical breakdown, the focal volume inside dielectric medium is changing rapidly towards the metal-like material since the free electron density becomes high (the bulk ripples are formed at $\sim 10^{18} - 10^{19}$ cm^{-3}). The corresponding dielectric function of focal region experience strong changes[17,18] and recording of ripples inside the volume can be considered as writing on the surface of a newly formed surface with different dielectric properties. At the dielectric breakdown (electron density $\sim 10^{21}$ cm^{-3} at the near-IR wavelengths) the ripples are not formed in the bulk.[19] This is caused by the sphere-to-plane transformation of nano-plasma bubbles inside the dielectric material which grow in the axial plane along the incident field for the in-bulk ripples (at the electron density $\sim 10^{18}$ cm^{-3}) and laterally at $\sim 10^{21}$ cm^{-3}.[20]

Further author information:
E-mail: rbuividas@swin.edu.au (R.B.), dday@swin.edu.au (D.D), sjuodkazis@swin.edu.au (S.J.).Tel.: (+61 3) 9214 8718, Fax: (+61 3) 9214 5435.

Plasmonics: Metallic Nanostructures and Their Optical Properties X, edited by Mark I. Stockman,
Proc. of SPIE Vol. 8457, 845728 · © 2012 SPIE · CCC code: 0277-786/12/$18 · doi: 10.1117/12.929574

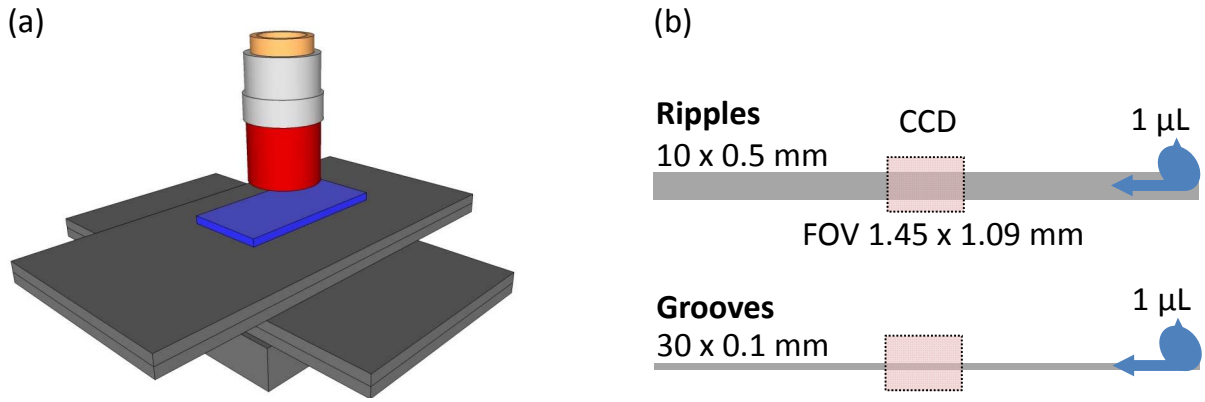

Figure 1. (a) Femtosecond laser pulse (800 nm / 150 fs) were introduced into an objective lens of numerical aperture $NA = 0.14$ (Mitutoyo) and focused onto sample which was on 3-axis linear positioning stages (Aerotech). (b) Setup used for monitoring water drag on ripples and grooves. CCD camera with 320×240 pixels for imaging at 25 fps was used with the same objective lens; CCD field of view $FOV = 1.45 \times 1.09$ mm^2 is indicated by the dashed line. Water droplet of 1 μl was placed at the end of the structure and monitored at the center (the FOV region).

When surface has structures which can couple an incoming light (usually at normal incidence) to the surface wave, a surface plasmon polariton (SPP), the ablated surfaces reveal the periodic SPP pattern as ripples. This is a special case of interaction of incoming light with surface wave derived for a general case in ref.[7,8] Very simple expressions are useful to estimate ripple period in the case of SPP:[21]

$$\Lambda_R = \lambda_0 \sqrt{\frac{\varepsilon_m + \varepsilon_d}{\varepsilon_m \varepsilon_d}}, \tag{1}$$

where λ_0 is the incident wavelength in air/vacuum and $\varepsilon_{m,d}$ are the real parts of the dielectric function of metal and dielectric, respectively (for notation: $\varepsilon \equiv n^2 = \varepsilon_1 + i\varepsilon_2$ when the refractive index is $n = n_1 + in_2$ and $\varepsilon_1 = n_1^2 - n_2^2$, $\varepsilon_2 = 2n_1 n_2$). For example, ripples on nickel $\varepsilon = n^2 = (2.48 + 4.38i)^2$ would predict $\Lambda_R = 769$ nm in air and 559 nm in water ($n_1 = 1.33$) for the incident wavelength $\lambda_0 = 800$ nm. These Λ_R values are close to the wavelength of incident light $\propto \lambda_0/n_1$ in the medium of propagation (with refractive index of n_1) and is typically observed on the ablated absorbing materials. Locations of the SPP crests on the plasmon supporting surface are the expected surface ablation places where ripple pattern is formed.

Here we investigate a recently reported phenomenon of superwicking surface modification of silicon.[22] We studied how shallow ripples made by fs-laser ablation can guide water micro-flow on the surface of silicon. The ripples were made at irradiance just slightly above the ablation threshold in order to avoid melt-overcast ridges and ablation of few-micrometer-deep grooves. Orientation of ripples in respect to the direction of the formed channel provides control of the flow rate. It was found that the nano- and micro-debris resulting from ablation is beneficial to droplet movement over the fabricated regions. Such "flat" ripple patterns have not been used before to guide water flow on surfaces. We use silicon as a prototype material in micro-chip fabrication where the water droplets can be used for self-assembly and alignment of micro-chips in industrial applications. Also, ripple formation on dielectric sapphire and transparent conductor of indium tim oxide (ITO) are demonstrated as promising platforms for optofluidic application in sensing.[23,24]

2. MATERIALS AND METHODS

We first describe ripple fabrication on silicon, sapphire and a thin ITO layer coated over a borosilicate glass using femtosecond laser pulses; then, water flow speed measurements on silicon ripples and grooves. The surface enhanced Raman scattering (SERS) measurements of a surface assembled monolayer (SAM) of thiophenol on the sapphire ripples was used to benchmark the substrate against those commercially available; and finally, electrical resistivity measurements on ITO surfaces patterned by ripples are presented.

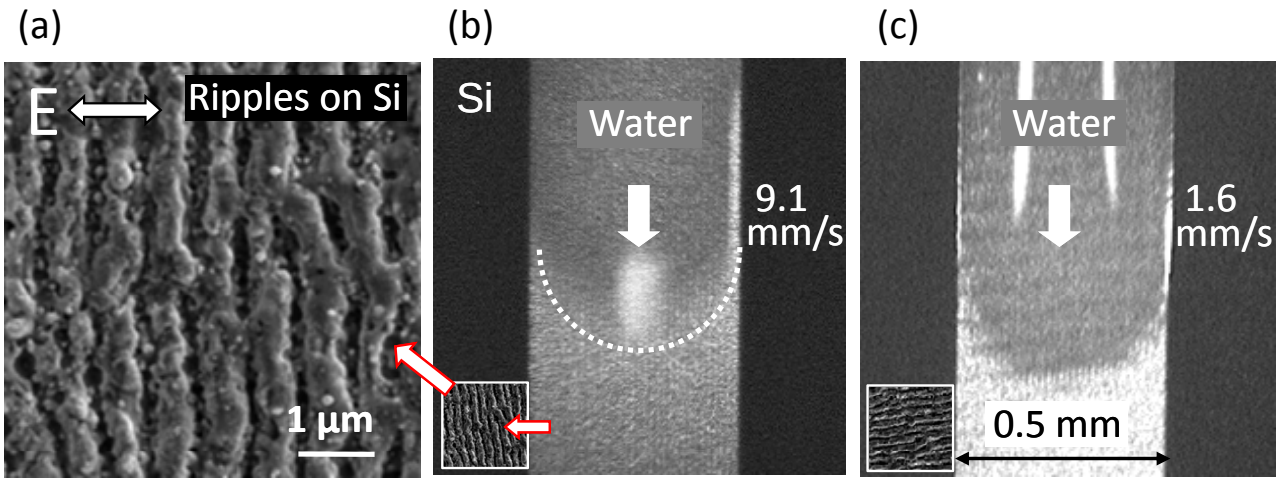

Figure 2. (a) SEM image of ripples on the Si substrate fabricated by femtosecond pulses. Polarization orientation of the laser beam is marked by an arrow. (b) Snap shot of a water droplet traveling on the ripples at 9.1 mm/s speed, when ripples were oriented parallel (see SEM image in the inset) to the water drag direction; white dashed line indicate the water front. (c) Snap shot of a water droplet traveling on the ripples at 1.6 mm/s speed, when ripples were oriented perpendicular (see inset) to the water drag direction. In both cases (b,c) width of fabricated area was 0.5 mm; white arrows show direction of the water drag.

2.1 Ripple fabrication

Ripple fabrication on silicon, sapphire and 45 nm thickness ITO layer on glass was performed using a regeneratively amplified Ti:Sapphire femtosecond laser system (Spitfire, Spectra Physics Inc.) operating at 800 nm central wavelength with a pulse duration of 150 fs, and repetition rate of 1 kHz. Ripples were fabricated in open air conditions using a linearly polarized laser radiation. Long working distance objective lenses (Mitutoyo Ltd.) were used to focus short laser pulses on the surface of substrates. High precision linear stages (Aerotech Inc.) were used to move the sample with respect to the focal spot of the laser beam (Fig. 1).

Ripples on a polished Si substrate were fabricated using a low numerical aperture $NA = 0.14$ objective lens in order to speed-up fabrication on a 10×0.5 mm^2 area. Whole area was fabricated by scanning parallel 10-mm-long lines with a $\sim$30% overlap; distance between lines was set to 7.5 μm, since measured line width was around 9 μm. Scan speed was 1 mm/s. Ripples oriented parallel and perpendicular to the channel structure were fabricated by rotating scan direction by 90° (Fig. 2). Pulse energy was set at $\sim$ 10% above the threshold for a single line fabrication(ablation) at the given speed. Groove on silicon substrate was fabricated using the same objective lens, scan speed was increased to 2 mm/s and pulse energy was by 70 times larger. Polarization was set along the scan line.

Ripples on a 400 μm thick high purity optical grade sapphire were fabricated over a 50×50 μm^2 area using a high numerical aperture $NA = 0.7$ objective lens. Parallel lines with a $\sim$ 30% overlap (line width 1 μm, distance between lines 0.7 μm) were fabricated to make a uniform area filled with ripples. Sample was moved at 10 μm/s speed, which resulted in $\sim$100 pulses overlap over spot size. Nitrogen gas was blown to prevent debris from accumulating on the sample surface during fabrication. Remaining debris were cleaned in a sequence in acetone, ethanol and high purity water for 2 min in each solution using an ultrasonic bath.

The same numerical aperture $NA = 0.7$ objective lens was used to fabricate uniform 50 $\times$50 μm^2 ripple area on a $t = 45$ nm thickness ITO layer deposited on a borosilicate cover glass (sheet resistance was $R_s = 100$ Ω/sq). At 4 μm period between lines, rippled grid pattern was fabricated. For larger area 1×1 mm^2 ripple fabrication $NA = 0.14$ objective lens was used with a 70 μm/s scan speed and a 4.5 μm period between lines. All samples were characterized by scanning electron microscopy (SEM).

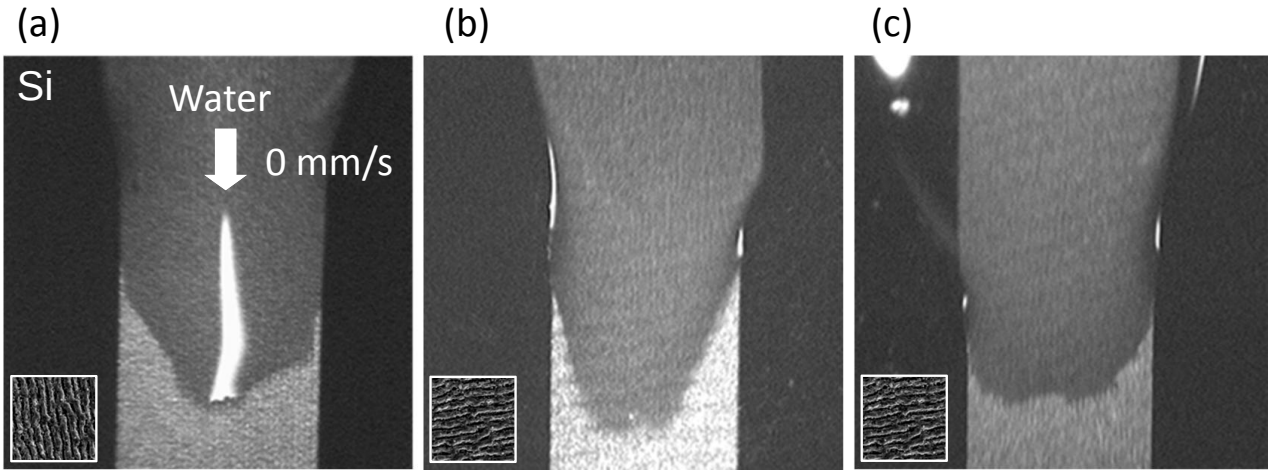

Figure 3. Edges of water droplet on the Si ripples after washing the laser fabrication debris in an ultrasonic bath: (a) when ripples oriented parallel and (b,c) perpendicular to the channel (see insets). (b) and (c) are the opposite sides of the same droplet.

2.2 Water flow speed measurement

For the experiments of water droplet flow over ripples we used deionized water of typical $\rho = 6$ MΩ·cm resistivity. Speed of a 1 μl droplet of deionized water was monitored at the center of channels fabricated on Si substrate using a 320×240 pixels, at 25 frames per second (fps) rate on CCD detector (Fig. 1 (b)). A $10\times$ magnifying objective lens (Mitutoyo) was used in combination with a 20 cm focal length tube lens to get a 1.45×1.09 mm^2 field of view (FOV) image on the CCD detector. Water flow speed was calculated from the video image sequence taken at 25 fps.

2.3 SERS measurement

Ripples on sapphire were coated by 400 nm gold using thermal vacuum evaporator (Emitech K950X, Quorum Technologies Ltd). The thickness of the metal layer was controlled by a quartz crystal thickness monitor. SERS spectra were measured using an In-Via Raman microscope (Renishaw Plc.). A He-Ne laser operating at $\lambda_{ex} = 633$ nm wavelength was used for the SERS excitation. A $20^{\times}$ objective lens with numerical aperture $NA = 0.4$ was used to focus the excitation laser beam and to collect Raman spectra in back-reflection. Signal was collected by a CCD detector after scattered light was dispersed by a 1800 lines/mm grating.

Ripples on sapphire and commercial SERS substrates (Solas and Klarite) were coated with a monolayer of thiophenol molecules C_6H_5SH (99%+, Sigma Aldrich) by immersing them in a 10 mM ethanol solution for 30 min followed by a rinse in ethanol. Thiophenol molecules are often used to study SERS enhancement, because they provide a strong Raman signal and form a stable self assembled monolayer (SAM) with surface coverage of 4.4×10^{-10} mol/cm^2 when deposited on the gold surface.[25]

Commercial SERS substrates (Solas and Klarite) were used as received with no extra treatment before depositing thiophenol molecules. Klarite SERS substrates (Renishaw Plc.) are fabricated using conventional optical lithography followed by anisotropic etching of a silicon wafer in KOH, which creates an array of inverted square pyramidal pits with a 2 μm period and 0.7-1 μm depth. A layer of gold ~300 nm thick is deposited on the substrate.[26] Another SERS substrate (Solas, API Defence Inc.) is fabricated on a base of 1-D silica grating produced by holographic lithography on silicon wafers. To reduce gaps in the silica grating it is overcoated with an additional layer of silica using plasma-enhanced chemical vapor deposition (PECVD). A 120 nm gold layer is deposited on the substrate.[27] Commercial SERS substrates' fabrication steps and conditions were described to explain the underlying principles according to the available literature.[26,27]

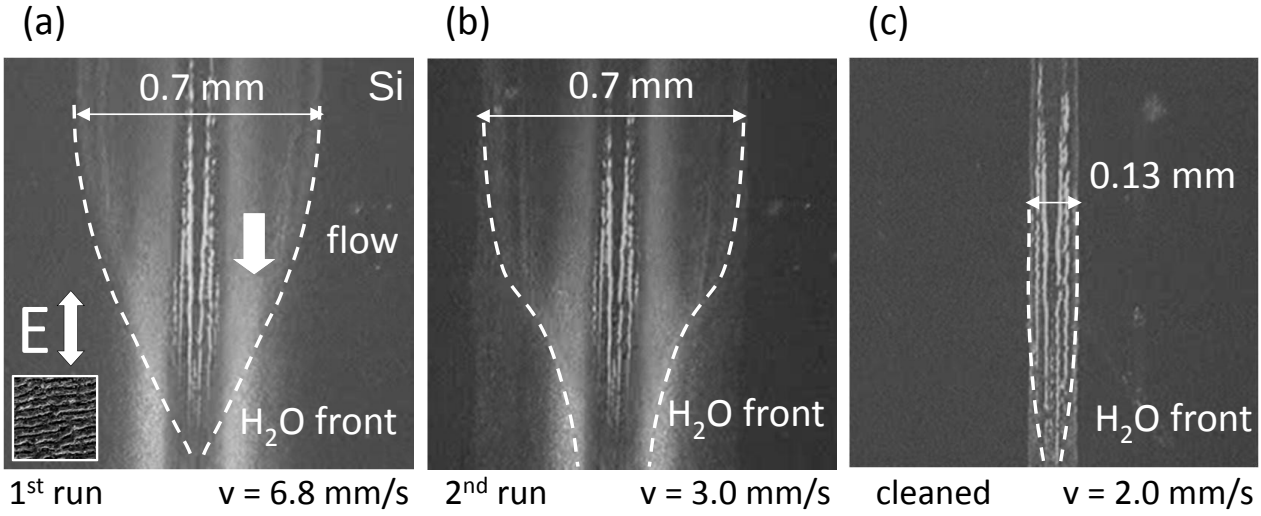

Figure 4. Snap shot of water droplet drag on a 0.13 mm wide groove fabricated on a Si substrate: (a) during the first and (b) second droplet flow and (c) after washing off fabrication debris in an ultrasonic bath. Length of all channels was 30 mm and snapshot was taken in the middle of the channel. Water was dragged at 6.8, 3.0 and 2.0 mm/s speed, respectively (shown in the panels).

2.4 Electrical resistance measurement

Electrical resistance on ripple-textured ITO layer was measured by an electrical needle-probes using a digital multimeter. Since the sheet resistance of the ITO film was comparatively low $R_s = \rho/t = 100\ \Omega/\text{sq}$ (conductivity $\propto 1/\rho$ is high), the errors introduced by the contact resistance were negligible.

3. RESULTS AND DISCUSSION

3.1 Water flow on Si ripples

Orientation of ripples on a Si substrates influences speed of water flow along the fabricated channel. Ripples, oriented parallel to the channel, drag water more than 5 times faster as compared to the perpendicularly oriented ripples (Fig. 2). Ripples of a 670 nm period on Si were fabricated using fs-laser pulses on a 10×0.5 mm^2 area. Orientation of ripples is controlled by polarization of the laser pulse (shown in the SEM image in Fig. 2(a) where polarization direction is indicated by an arrow). Figures 2(b) and (c) show snap shots of a 1 μl droplet of a deionized water front moving over the ripple textured channel. Water traveled at a 9.1 mm/s speed, when ripples were oriented along the channel and at 1.6 mm/s, when ripples were perpendicular to the channel/flow. Direction of ripples is shown in SEM images in the insets. In both cases there was no surface cleaning used after laser ablation, hence, a nano- micro-particulates of silica and silicon were present on the surface.

After the samples were washed in an ultrasonic bath the water droplet showed an initial spreading along the ablated surface, but was not moving as on the as-ablated surface (Fig. 3). Interestingly, a slightly more elongated droplet was formed when ripples were oriented perpendicular to the channel (b). A contact angle of the water droplet should be measured[3] in order to judge on the wettability change and is planed in future work. Length of the droplet was 3-4 mm. Apparently, removal of silica particulates which are hydrophilic changed the water droplet movement over ablated regions. Arguably, the presence of debris on the laser treated surfaces might significantly contribute to the formation of a super-wicking surface reported recently.[22]

The flow speed of water droplet on the flat areas covered by ripples was compared to the water flow speed in a grove-channel, fabricated by femtosecond laser pulses on the same Si substrate. The fabricated groove-channel is shown in Fig. 4, polarization direction was set along the grove during fabrication, so, ripples are formed on the side walls of the groove are oriented perpendicular to the grove. A 1 μl water droplet was dropped at the end of the fabricated region and quickly spread all over the groove with water front speed observed on the CCD field of

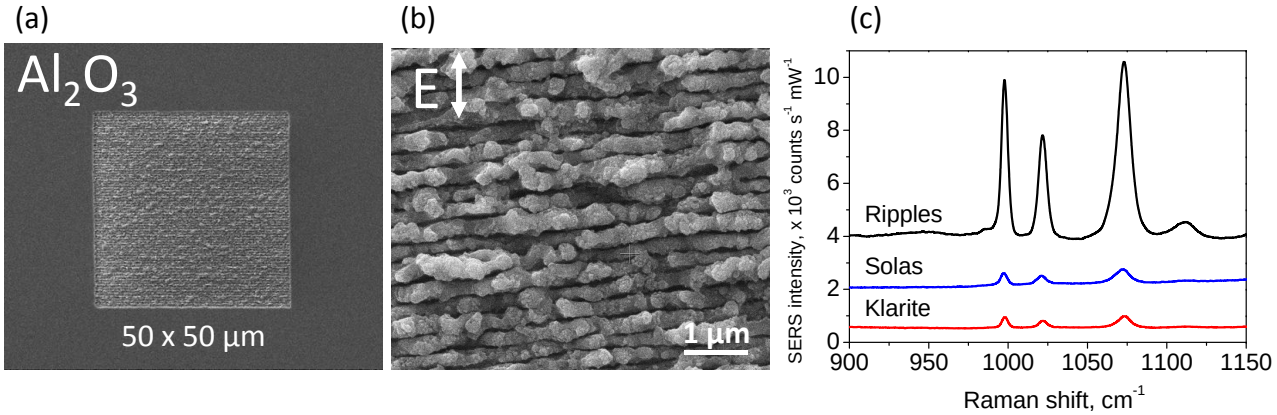

Figure 5. (a) SEM image of ripples fabricated on 50×50 μm area on a Al_2O_3 substrate by femtosecond pulses. (b) A zoomed-in region of the ripples, polarization direction of the fabrication laser beam indicated by an arrow. (c) SERS spectra of thiophenol monolayer measured using 633 nm, 10 mW He-Ne laser for excitation. Ripples on Al_2O_3 coated with 400 nm Au by magnetron sputtering and their sensitivity compared with commercial SERS substrates Solas and Klarite; note, Klarite substrates are coated with ~ 300 nm, Solas with 120 nm gold layer. Only 30 nm of gold is required on ripples to achieve sensitivity of commercial substrates.

view equal to $v \simeq 6.8$ mm/s. If we compare this speed with the one for the same ripple direction (perpendicular to water flow), water droplet traveled faster in the groove as compared with the flat rippled surfaced by a factor of ~ 4, corroborating the super-wicking effect.[22] However, water was traveling 1.3 times faster on the flat surface ripples when they were aligned along the flow. Water front is shown in Fig. 4 by a dashed line. Water was flowing faster in the groove dragging the droplet over a several times wider debris region (see, panels (a) and (b)). Second run of the droplet was approximately twice slower, but also it was spread along the entire channel. After surface cleaning in ultrasonic bath, the droplet transport was pinned to the laser ablated groove only, was spreading slower and was not reaching the end of the ablated region. This is consistent with the droplet transport on the flat ripples' channel (Figs. 2-4).

3.2 SERS on Al_2O_3 ripples

Ripples, fabricated on sapphire substrate and coated by 400 nm Au layer, have 13 and 15 times higher sensitivity compared to commercial SERS substrates Klarite and Solas, respectively (Fig. 5). A 50×50 μm^2 size area of ripples was fabricated, which is considered large enough for SERS measurement using a microscope type Raman measurement system. Semi-periodic structure of ripples is revealed under SEM images (Fig. 5 (a),(b)). Typical thiophenol spectra are presented in Fig. 5(c) with the bands at 998, 1022 and 1073 cm^{-1} assigned to the in-plane ring-breathing mode, the in-plane C-H bend, and the in-plane ring-breathing mode coupled to the ν(C-S) mode, respectively.[28] The band frequencies are slightly shifted from those of a pure thiophenol, which is well known to happen due to the molecule binding to the metal substrate.[29] Sensitivity of the substrates was compared by measuring average peak height values of three thiophenol peaks at 998, 1022 and 1073 cm^{-1}. This provides a single reliable value representing the SERS signal intensity and hence can be used to compare sensitivity between different SERS substrates. The maximum peak heights were measured relative to the background level, given by a third order polynomial function fitted to selected spectral regions away from the peaks (928-988, 1007, 1033 - 1049, 1036 cm^{-1}).

The SERS intensity of thiophenol SAM depends on the thickness of the deposited Au layer on the ripples. The SERS signal is higher for thicker coatings at least up to 400 nm, showing a slight tendency towards saturation. Thicker coatings are not practical and have not been tested. SERS intensity scales linearly with the excitation power on ripples coated with gold. Very low power of 10 μW was sufficient to get a reasonable SERS signal using ripples coated by 135 nm Au, with a noise to signal ratio $\sim$2.5. For thicker coatings even lower power would be sufficient. The reproducibility of SERS signal on ripples was compared with Klarite substrate. Reproducibility is the second most important parameter after the enhancement or sensitivity of the SERS substrate, especially

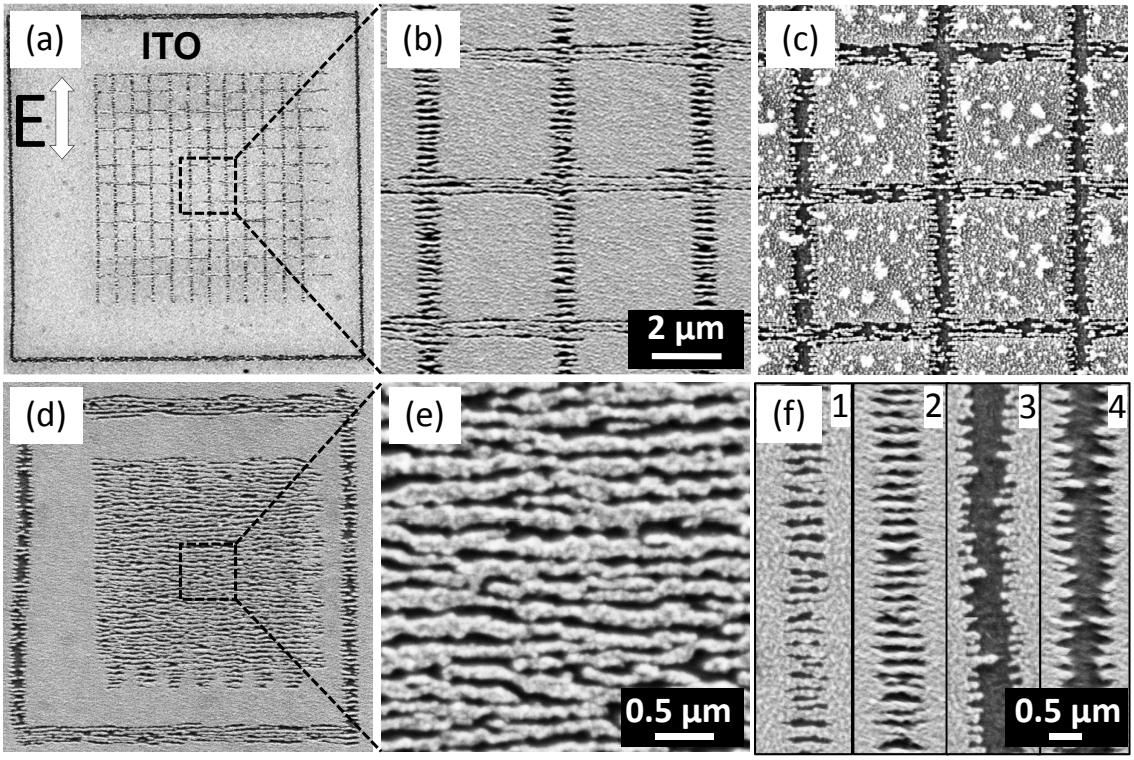

Figure 6. SEM images of ripples, fabricated on a $t = 45$ nm-thick ITO film on glass (sheet resistance $R_s \equiv \rho/t = 100\ \Omega$/sq) focusing 150 fs pulses at 800 nm wavelength with $NA = 0.7$ objective. Ripples with period of ∼150 nm were formed under back side irradiation, focusing through a cover glass on the ITO layer (c). Under front side laser irradiation ∼200 nm period ripples were formed (all except c). Same scale used for (a) and (d) images, outer frame size is 1×1 mm. Distance between lines is 4 μm for (b,c) and 0.7 μm for (e). Ripples fabricated at different pulse energy 31, 35, 39, 42 nJ, numbered 1 - 4 respectively, (f). Images of all samples except (c) were taken after washing samples in ultrasonic bath.

for practical applications.[30] Signal uniformity depends on the numerical aperture of the objective used to excite and collect Raman signal, since it defines the area from where signal is measured. For high numerical aperture $NA = 0.75$ objective lens, theoretically estimated Gaussian beam focal spot diameter ($d = 1.22\lambda/NA$) was equal to ~ 1 μm. In this case, relative standard deviation (RSD) of the SERS intensity $RSD = 10$ % was more than two times smaller than that of Klarite $RSD = 24$ %. The RSD of signal was calculated from more than 100 spots on each of the samples. For a lower numerical aperture ($NA = 0.4$) objective lens, estimated spot size was equal to 2 μm and the RSD of the Klarite substrate decreased to 14 %, while remaining unchanged for the ripples.

Ripple fabrication is a flexible surface nanotexturing technique, where surface parameters can be easily modified. Period of the ripples can be tuned by the wavelength of fabrication laser or material used, depth and width of the grooves can be tuned by scanning algorithm and deposited laser intensity. Direction of the ripples is controlled by polarization direction. Nanoscale roughness on the ripples depend on a fabrication laser intensity and post processing treatment, e.g. chemical or plasma etching.

Metal nano-feature size on the ripples can be controlled by deposition techniques and parameters or post processing, e.g. thermal annealing and Oswald ripening which control size of spheroidal nanoparticles. Different metals can be coated on the ripples to shift plasmon resonance to the required excitation wavelength, e.g. to benefit from resonant SERS (SERRS), where signal is at least few orders of magnitude larger. The measured optical extinction spectra of the ripples on sapphire coated by 30 nm of gold (not shown here), was reaching 0.4 over 550-700 nm range popular in Raman measurements. An interplay between absorption and scattering (together they constitute extinction) by a nanoparticle size provides ways to tune the extinction spectra and

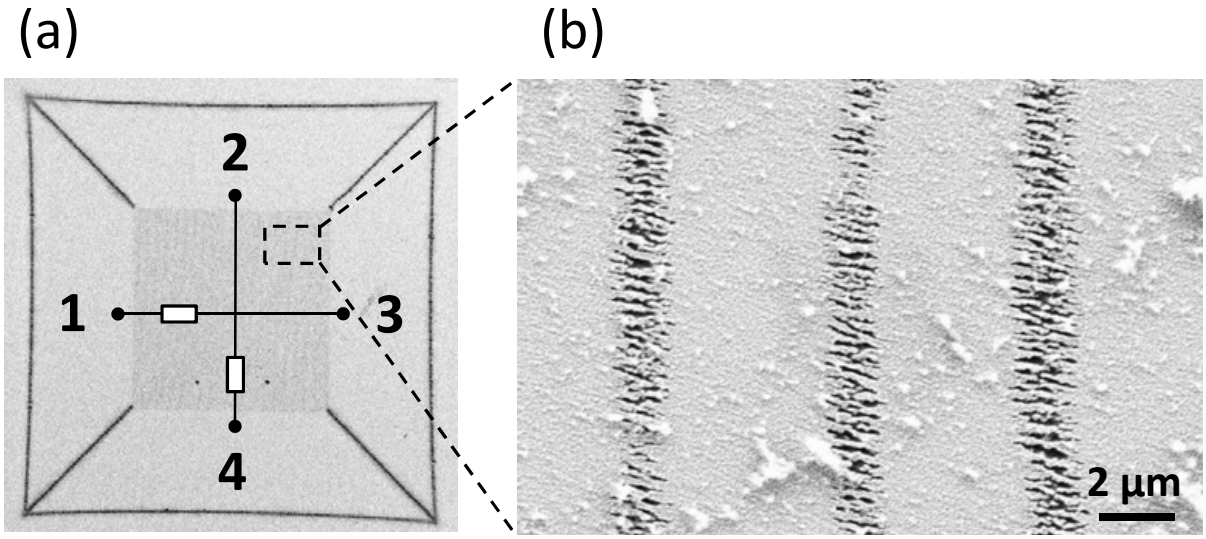

Figure 7. Resistance was measured of the isolated (from the rest of the ITO sheet) ITO pads which were separated by the ripple-textured ITO regions. Resistance along and across ripples' orientation is changed 3 times.

optical properties of nano-textured surfaces. Indeed, the absorption cross section scales as $C_{abs} \propto V$ while scattering as $C_{sc} \propto V^2$ with volume, V. This is determined by a generic dependence of cross sections on polarizability, $\alpha \propto r^3$ (for the spherical particles of radius, r):[31]

$$C_{abs} = k\mathrm{Im}(\alpha), \tag{2}$$

$$C_{sc} = \frac{k^4}{6\pi}|\alpha|^2 \tag{3}$$

where k is the wavevector and polarizability is given by $\alpha = 4\pi r^3 \frac{\varepsilon_m - \varepsilon_d}{\varepsilon_m + 2\varepsilon_d}$. Hence, via the particle size on ripples, the scattering or absorption can be favored in the extinction spectrum when required for sensing and light harvesting applications.

Direct laser writing of ripples is less complicated and also less expensive as compared to commercial SERS substrates' fabrication, where optical lithography, chemical or plasma etching and PECVD were used. Higher sensitivity, better reproducibility, lower cost of fabrication and flexible tuning of surface parameters are the main reasons why ripples are promising as new commercial SERS substrates.

Ripples on Si substrates were demonstrated as a SERS platform. However, there is little control over the surface morphology when ripples are formed on the absorbing surfaces. The period of the ripples is close to the wavelength (see, eqn. 1) and although it can be reduced by using a slanted incidence or liquid ambient (eqn. 1), however, this comes at the expense of a more complex and less efficient (due to stronger reflection) fabrication method.

3.3 Ripples on ITO layer

Ripples on ITO layer of only 45 nm thickness were formed by top and back side irradiation. Figure 6 shows typical morphology of ripples formed on ITO film. In case of the front side illumination, experimentally observed period of the ripples was about 200 nm, while at the back side illumination – 150 nm (Fig. 6). The expected period for the ripple recording at tight focusing via sphere-to-plane sub-surface breakdown[20] is $\lambda_0/n_{ITO}/2 \simeq 225$ nm for the front side irradiation and $(\lambda_0/n_{BK7})/n_{ITO}/2 \simeq 150$ nm for the back side irradiation. $n_{ITO} = 1.78$ is the refractive index of ITO and $n_{BK7} = 1.51$ is the refractive index of borosilicate glass at 800 nm wavelength. In both cases the theory of half-wavelength cavity feedback[20] closely predicts / explains the experimentally observed period of ripples.

Since ITO is conductive, one might expect to obtain the ripples close to the period of light wavelength as predicted by Sipe et al theory[7,8] or by SPP theory (eqn. 1); note Sipe's theory predict ripples of λ_0/n when $n \approx 1$.[12] The dielectric function of ITO at 800 nm is $\varepsilon = (1.76447 + 8.2831i \times 10^{-2})^2$, hence, one would find $\Lambda_R = 700$ nm for the glass|ITO boundary and $\Lambda_R = 920$ nm for the ITO|air surface according to the SPP model (eqn. 1). Predicted values are far from experimentally obtained ones, which suggests that Sipe et al theory[7,8] and specialized SPP case can not explain ripples formation on thin ITO coatings.

The back-side mode of laser ablation is preferable since smaller period ripples can be formed. As well, it is beneficial since debris have momentum along the beam propagation which helps to remove particulates better. Period of the ripples did not depend on laser pulse energies in the range between $E_p = 30 - 40$ nJ and was about 190 - 210 nm (Fig. 6(f)). Higher energy range was not tested because ITO was completely removed at $E_p > 40$ nJ. It was found that fabrication speed did not influence the period. Ripples fabricated at 10 μm/s speed (Fig. 6(a,d)), and at 70 μm/s (f) had same period $\sim$200 nm; pulse overlap over the focal spot area was about 80 and 11, respectively.

Amount of ITO removed by ripple pattern in a single line/scan can vary with laser power. It is possible to remove all the ITO layer by ablation leaving glass surface exposed. This entitles to use direct writing approach to free form writing of contacts and design freely patterns which can be electrically connected, e.g, a heater meandering line or interdigitated contacts can be writen onto the substrate. This is promising in micro-fluidic chemical reactors, sensors,[23,24] and can find applications in opto-mechanical applications based on laser tweezers.[32–39] The smallest feature sizes of single holes ablated by single fs-laser pulses was equal to the typical grain size of the ITO film and was approximately 20-30 nm (not shown here). Laser power necessary to ablate thin film is compatible with that provided by simpler fs-laser oscillators (without regenerative amplifiers).[32,40–42]

Figure 7 shows pattern of ripples which was used to modify resistance as it was measured along and across the ripples from isolated contact pads (contact resistance was small). The difference in resistance was three times. On such patterned electrodes, wetting can be additionally controlled via electrowetting mechanism and could also be used in control of liquid spreading over ripple-textured surface discussed above for silicon.

4. CONCLUSIONS AND OUTLOOK

Orientation of ripples is shown to affect the water droplet spreading on the surface of silicon. Difference up to 6 times in the water spreading speed has been detected on the flat ripples covered regions. Laser ablated grooves (with ripples) showed faster water spreading, however, the volume of removed material and overcasted debris was considerably more significant as compared with the flat-rippled patterning of surfaces.

We showed that presence of hydrophilic debris of nano-micro-particles has a strong effect on the water spreading over ablated surfaces and ablated grooves. This is an important factor in explanation of the superwicking surface effect on silicon formed by fs-laser ablation.[22] Ripples can simultaneously deliver liquid solution and facilitate sensing/detection of analyte, e.g., using SERS. Ripples on sapphire were demonstrated to have more than 10 $\times$ times better sensitivity and superior reproducibility as compared to commercial SERS substrates. Wetting conditions of surfaces and changes between the Cassie-Baxter and Wenzel mechanism using ripples can be foreseen and requires future research.

Patterned electrodes with nano-features of tens-of-nanometers acts as lighting rod for the electrical field applied electrically or optically. This synergy is promising in future sensing applications. One more promising field of application is creation of liquid crystal panels with the laser patterned ITO electrodes for controlling propagating light front and phase. Such devices, are used in quantum computing (so called q-plates) and in laser machining as diffractive optical elements which can substitute expensive spatial light modulators.

ACKNOWLEDGEMENTS

Partial financial support by an Agilent and Australian Research Council DP120102980 grants is acknowledged. We are grateful to Tecdia Inc. Japan for sapphire samples and acknowledge discussion with Dr. James Chon on optical properties of nanoparticles.

REFERENCES

[1] Birnbaum, M., "Semiconductor surface damage produced by ruby lasers," *J. Appl. Phys.* **36**(11), 3688 (1965).

[2] Emmony, D. C., "Laser mirror damage in germanium at 10.6 μm," *App. Phys. Lett.* **23**(11), 598 (1973).

[3] Wu, B., Zhou, M., Li, J., Ye, X., Li, G., and Cai, L., "Superhydrophobic surfaces fabricated by microstructuring of stainless steel using a femtosecond laser," *App. Surf. Sc.* **256**(1), 61–66 (2009).

[4] Bizi-Bandoki, P., Benayoun, S., Valette, S., Beaugiraud, B., and Audouard, E., "Modifications of roughness and wettability properties of metals induced by femtosecond laser treatment," *Appl. Surf. Sc.* **257**(12), 5213–5218 (2011).

[5] Chen, J.-T., Lai, W.-C., Kao, Y.-J., Yang, Y.-Y., and Sheu, J.-K., "Laser-induced periodic structures for light extraction efficiency enhancement of GaN-based light emitting diodes.," *Opt. Express* **20**(5), 5689–95 (2012).

[6] Halbwax, M., Sarnet, T., Delaporte, P., Sentis, M., Etienne, H., Torregrosa, F., Vervisch, V., Perichaud, I., and Martinuzzi, S., "Micro and nano-structuration of silicon by femtosecond laser: Application to silicon photovoltaic cells fabrication," *Thin Solid Films* **516**(20), 6791–6795 (2008).

[7] Young, J., Preston, J., Van Driel, H., and Sipe, J., "Laser-induced periodic surface structure. II. Experiments on Ge, Si, Al, and brass," *Phys. Rev. B* **27**(2), 1155–1172 (1983).

[8] Sipe, J., Young, J., Preston, J., and Van Driel, H., "Laser-induced periodic surface structure. I. Theory," *Phys. Rev. B* **27**(2), 1141–1154 (1983).

[9] Juodkazis, S., Nishimura, K., Okuno, H., Tabuchi, Y., Matsuo, S., Tanaka, S., and Misawa, H., "Three-dimensional laser microfabrication of metals, semiconductors, and dielectrics," in [*ProcP SPIE*], **6732**, 67320B (2007).

[10] Juodkazis, S., Tabuchi, Y., Ebisui, T., Matsuo, S., and Misawa, H., "Anisotropic etching of dielectrics exposed by high intensity femtosecond pulses," in [*Proc. SPIE*], **5850**, 59 (2005).

[11] Louchev, O., Juodkazis, S., Misawa, H., and Kitamura, K., "Formation of nanofibers and microspheres by femtosecond laser ablation of chalcogenide glasse," in [*Proc. SPIE*], **6732**, 673210 (2007).

[12] Iwase, H., Kokubo, S., Juodkazis, S., and Misawa, H., "Suppression of ripples on Ni surface via a polarization grating," *Opt. Express* **17**(6), 4388–4396 (2009).

[13] Juodkazis, S., Kujime, N., Okuno, H., Mizeikis, V., Matsuo, S., and Misawa, H., "Towards nanostructuring of materials by ripples," in [*Proc. of Joint Int. Workshop CREST& QNN*], **3**, 21–23 (2003).

[14] Shimotsuma, Y., Kazansky, P., Qiu, J., and Hirao, K., "Self-organized nanogratings in glass irradiated by ultrashort light pulses," *Phys. Rev. Lett.* **91**(24), 247405 (2003).

[15] Bhardwaj, V., Simova, E., Rajeev, P., Hnatovsky, C., Taylor, R., Rayner, D., and Corkum, P., "Optically Produced Arrays of Planar Nanostructures inside Fused Silica," *Phys. Rev. Lett.* **96**(5), 1–4 (2006).

[16] Richter, S., Heinrich, M., Döring, S., Tünnermann, A., Nolte, S., and Peschel, U., "Nanogratings in fused silica: Formation, control, and applications," *J. Las. Appl.* **24**(4), 042008 (2012).

[17] Juodkazis, S., Nishimura, K., and Misawa, H., "In-bulk and surface structuring of sapphire by femtosecond pulses," *Appl. Surf. Sci.* **253**(15), 6539 – 6544 (2007).

[18] Juodkazis, S., Nishimura, K., and Misawa, H., "Three-dimensional laser structuring of materials at tight focusing," *Chin. Opt. Lett.* **5**, S198 – 200 (2007).

[19] Kudrius, T., Šlekys, G., and Juodkazis, S., "Surface-texturing of sapphire by femtosecond laser pulses for photonic applications," *J. Phys. D: Appl. Phys.* **43**(14), 145501 (2010).

[20] Buividas, R., Rosa, L., Šliupas, R., Kudrius, T., Šlekys, G., Datsyuk, V., and Juodkazis, S., "Mechanism of fine ripple formation on surfaces of (semi) transparent materials via a half-wavelength cavity feedback," *Nanotechnology* **22**, 055304 (2011).

[21] Raether, H., [*Surface plasmons on smooth and rough surfaces and on gratings*], Springer-Verlag (1988).

[22] Vorobyev, A. Y. and Guo, C., "Laser turns silicon superwicking," *Opt. Express* **18**(7), 6455–6460 (2010).

[23] Misawa, H. and Juodkazis, S., "Photophysics and photochemistry of a laser manipulated microparticle," *Prog. Polym. Sci.* **24**, 665–697 (1999).

[24] Islam, M. M., Ueno, K., Juodkazis, S., Yokota, Y., and Misawa, H., "Development of interdigitated array electrodes with SERS functionality," *Analytical Sciences* **26**, 13–18 (2010).

[25] Sawaguchi, T., Mizutani, F., Yoshimoto, S., and Taniguchi, I., "Voltammetric and in situ STM studies on self-assembled monolayers of 4-mercaptopyridine, 2-mercaptopyridine and thiophenol on Au(111) electrodes," *Electrochimica Acta* **45**(18), 2861–2867 (2000).

[26] Perney, N. M. B., Baumberg, J. J., Zoorob, M. E., Charlton, M. D. B., Mahnkopf, S., and Netti, C. M., "Tuning localized plasmons in nanostructured substrates for surface-enhanced Raman scattering.," *Opt. Express* **14**(2), 847–57 (2006).

[27] Deng, X., Braun, G. B., Liu, S., Sciortino, P. F., Koefer, B., Tombler, T., and Moskovits, M., "Single-order, subwavelength resonant nanograting as a uniformly hot substrate for surface-enhanced Raman spectroscopy.," *Nano Lett.* **10**(5), 1780–6 (2010).

[28] Bryant, M. A., Joa, S. L., and Pemberton, J. E., "Raman scattering from monolayer films of thiophenol and 4-mercaptopyridine at platinum surfaces," *Langmuir* **8**(3), 753–756 (1992).

[29] Saikin, S., Olivares-Amaya, R., Rappoport, D., Stopa, M., and Aspuru-Guzik, A., "On the chemical bonding effects in the raman response: Benzenethiol adsorbed on silver clusters," *Phys. Chem. Chem. Phys.* **11**(41), 9401–9411 (2009).

[30] Brown, R. and Milton, M., "Nanostructures and nanostructured substrates for surface-enhanced Raman scattering (SERS)," *J. Raman Spectr.* **39**(10), 1313–1326 (2008).

[31] Okamoto, T., [], ch. Near-field spectral analysis of metallic beads, 98–123, Springer-Verlag, Berlin (2001).

[32] Vanagas, E., Kudryashov, I., Tuzhilin, D., Juodkazis, S., Matsuo, S., and Misawa, H., "Surface nanostructuring of borosilicate glass by femtosecond nJ energy pulses," *Appl. Phys. Lett.* **82**(17), 2901–2903 (2003).

[33] Juodkazis, S., Matsuo, S., Murazawa, N., Hasegawa, I., and Misawa, H., "High-efficiency optical transfer of torque to a nematic liquid crystal," *Appl. Phys. Lett.* **82**(26), 4657–4659 (2003).

[34] Brasselet, E., Murazawa, N., Misawa, H., and Juodkazis, S., "Optical vortices from liquid crystal droplets," *Phys. Rev. Lett.* **103**, 103903 (2009).

[35] Brasselet, E., Balčiūnas, T., Murazawa, N., Juodkazis, S., and Misawa, H., "Light-induced nonlinear rotations of nematic liquid crystal droplets trapped in laser tweezers," *Mol. Cryst. Liq. Cryst.* **512**, 1989–1997 (2009).

[36] Brasselet, E. and Juodkazis, S., "Optical angular manipulation of liquid crystal droplets in laser tweezers," *J. of Nonlin. Opt. Phys. and Mat.* **18**(2), 167–194 (2009).

[37] Brasselet, E., Murazawa, N., Juodkazis, S., and Misawa, H., "Statics and dynamics of radial nematic droplets manipulated by laser tweezers," *Phys. Rev. E* **77**, 041704 (2008).

[38] Juodkazis, S., Shikata, M., Takahashi, T., Matsuo, S., and Misawa, H., "Size dependence of rotation frequency of individual laser trapped liquid crystal droplets," *Jpn. J. Appl. Phys.* **38**, L518–520 (1999).

[39] Brasselet, E. and Juodkazis, S., "Intangible pointlike tracers for liquid-crystal-based microsensors," *Phys. Rev. A* **82**, 063832 (2010).

[40] Juodkazis, S., Mizeikis, V., and Misawa, H., "Three-dimensional microfabrication of materials by femtosecond lasers for photonics applications," *J. Appl. Phys.* **106**(5), 051101 (2009).

[41] Juodkazis, S., Mizeikis, V., Matsuo, S., Ueno, K., and Misawa, H., "Three-dimensional micro- and nanostructuring of materials by tightly focused laser radiation," *Bull. Chem. Soc. Jpn.* **81**(4), 411–448 (2008).

[42] Seet, K. K., Juodkazis, S., Jarutis, V., and Misawa, H., "Feature-size reduction of photopolymerized structures by femtosecond optical curing of SU-8," *Appl. Phys. Lett.* **89**, 024106 (2006).